Available online at www.sciencedirect.com
ScienceDirect
International Journal of Heat and Mass Transfer 50 (2007) 4845–4854
International Journal of HEAT and MASS TRANSFER
www.elsevier.com/locate/ijhmt

Heat transfer and friction characteristics for artificially roughened ducts with compound turbulators

Apurba Layek [a,*], J.S. Saini [b], S.C. Solanki [b]

[a] Department of Mechanical Engineering, NIT Durgapur 713 209, India
[b] Department of Mechanical and Industrial Engineering, IIT Roorkee 247 667, India

Received 15 May 2006; received in revised form 10 February 2007
Available online 12 June 2007

Abstract

An experimental investigation on heat and fluid flow characteristics of fully developed turbulent flow in a rectangular duct having repeated integral transverse chamfered rib-groove roughness on one broad wall has been carried out. Experiments encompassed the Reynolds number range of 3000–21,000; relative roughness pitch of 4.5–10, chamfer angle of 5°–30°, relative groove position of 0.3–0.6 and relative roughness height of 0.022–0.04. The effect of roughness parameters on Nusselt number and friction factor have been discussed and the results are compared with the results of square rib-grooved and smooth duct under similar flow conditions. The conditions for the best performance have been determined. Correlations for the Nusselt number and friction factor have been developed as a function of roughness parameters and flow Reynolds number.

Keywords: Compound-roughness; Heat transfer coefficient; Friction factor; Chamfer angle and groove position

1. Introduction

Use of artificial roughness in the form of repeated ribs has been found to be an efficient method of enhancing the heat transfer to fluid flowing in the duct. The application of artificial roughness in the form of fine wires and ribs of different shapes has been recommended to enhance the heat transfer coefficient by several investigators [3–5,7,8,10,13,14]. It has been found that the main thermal resistance to the convective heat transfer is due to the presence of laminar sub-layer on the heat-transferring surface. The ribs break the laminar sub-layer and create local wall turbulence due to flow separation and reattachment between consecutive ribs, which reduce the thermal resistance and greatly enhance the heat transfer. However, the use of artificial roughness results in higher friction and hence higher pumping power requirements. Therefore, it is desirable that the turbulence should be created in the vicinity of the wall, i.e. only in the laminar sub-layer region, which is responsible for thermal resistance. Hence, the efforts of researchers have been directed towards finding the roughness shape and arrangement, which break the laminar sub-layer, enhance the heat transfer coefficient most with minimum pumping power penalty. Nikuradse [9], Dipprey and Sabersky [1] developed a friction similarity law and a heat momentum transfer analogy for flow in rough tubes. Webb and Eckert [13] developed the heat transfer and friction factor correlations for turbulent air flow in tubes having repeated rib roughness. Han [4] carried out an experimental study for the fully developed turbulent airflow in square ducts with two opposite rib roughened walls. Liou and Hwang [7,8] utilized a real time Laser Holographic Interferometry [LHI] to measure the local as well as average heat transfer coefficient and compared the performance of square, triangular and semi-circular ribs and showed that the square ribs give best heat transfer performance among them. Zhang et al. [14] reported that the addition of grooves in between adjacent

* Corresponding author. Fax: +91 1332 285665.
E-mail address: apurba_layek@yahoo.co.in (A. Layek).

0017-9310/$ - see front matter © 2007 Elsevier Ltd. All rights reserved.
doi:10.1016/j.ijheatmasstransfer.2007.02.042

Nomenclature

A_p	absorber plate area (m^2)
C_p	specific heat of air (J/kg K)
D_h	hydraulic diameter (m)
e	rib height, groove depth (m)
e/D_h	relative roughness height
f	fanning friction factor
f_c	fanning friction factor for circular duct
G	mass velocity of air (kg/s m^2)
g	groove distance from rib centre line (m)
g/P	groove relative distance
H	duct depth (m)
h	heat transfer coefficient (W/m^2)
k	thermal conductivity of air (W/m K)
L_f	pressure taps distance (m)
$\dot{m}$	mass flow rate (kg/s)
Nu	Nusselt number, $=hD_h/k$
P	rib pitch
P/e	relative roughness pitch
Q_u	heat transfer rate (W)
Re	Reynolds number, $=GD_h/\mu$
T_{fm}	bulk mean air temperature $= T_o - T_i)/2$ (°C)
T_i	inlet air temperature (°C)
T_o	outlet air temperature (°C)
T_{pm}	mean plate temperature (°C)
W	width of the duct (m)
W/H	duct aspect ratio
δp	pressure drop through duct (Pa)
ρ	density of air (kg/m^3)
μ	dynamic viscosity of air (Pa s)
ϕ	chamfer angle (°)
β	ratio of orifice diameter to pipe diameter

Subscript

s	smooth duct

square ribs enhance the heat transfer capability of the surface considerably with nearly same pressure drop penalty. Most of these investigations have been conducted for a turbine blade cooling design to optimize the ridge geometry in order to obtain the best heat transfer coefficients for either a given cooling rate or an available pressure drop across the cooling passage. It has recently been proposed by several investigators that providing artificial roughness on the underside of its absorber plate could substantially enhance the heat transfer capability of a solar air heater. Prasad et al. [10] and Gupta et al. [3] carried out studies on rectangular duct with protrusion of circular wire roughness on the heated wall. Karwa et al. [5] experimented on integral chamfered rib-roughness on the heated wall. They reported that chamfer angle of 15° gives maximum heat transfer. It is reported by Webb and Eckert [13] that square ribbed surface having relative roughness pitch (P/e) less than 8 does not reattaches the free shear layer. While Zhang et al. [14] observed that deploying of groove in between the ribs enhances the turbulences as well as reattaches the free shear layer nearer to the rib. Chamfering the rib top also makes the reattachment of the flow further closer to the rib. It appears that it will be fruitful to investigate an artificially roughened surface with optimally chamfered rib combined with grooves present between two ribs in order to achieve further decrease in relative roughness pitch and enhancement of heat transfer rate from such a surface. In view of the above an experimental investigation has been planned to investigate the heat and fluid flow characteristics of artificially roughened surface with chamfered rib-grooved roughness. The details of the experimental set-up, data collection and processing and the results are being presented in the following sections.

2. Roughness geometry and range of parameters

Fig. 1 shows the general geometry of the roughened plate having artificial roughened in the form of chamfered repeated ribs with grooves in between the ribs. The cross section of roughness can be described by the values of rib height, e, rib pitch, P, chamfer angle, ϕ and groove position between the ribs, g. In this study the rib height equals the groove depth for the entire roughened surfaces. These parameters have been expressed in the form of the following dimensionless roughness parameters:

(i) Relative roughness pitch, P/e.
(ii) Relative roughness height, e/D_h.
(iii) Relative groove position, g/P.

The range of parameters for this study has been decided on the basis of practical considerations of the system and operating conditions of the solar air heater and is given in Table 1. The minimum rib height was chosen such that the laminar sub-layer would be of the same order as roughness height at the lower flow Reynolds number. The maximum rib height was 2 mm so that the flow passage blockage effects are negligible.

3. Experimental program

3.1. Experimental apparatus

The schematic diagram of the experimental set-up including the test section is shown in Fig. 2. The flow system consists of an entry section, an exit section, a flow meter and a centrifugal blower. The duct is 2600 mm long,

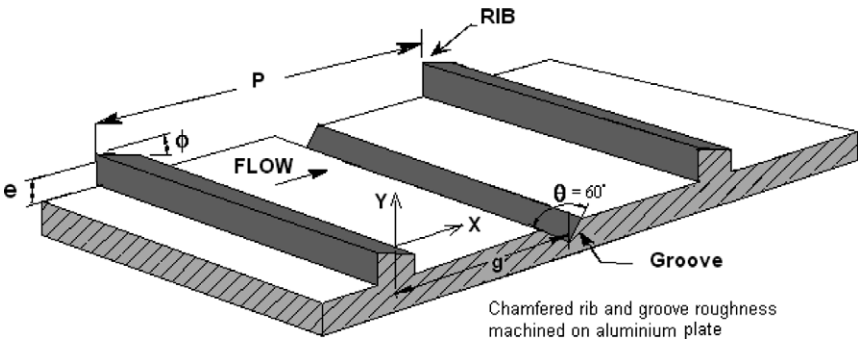

Fig. 1. Rib geometry.

Table 1
Range of parameters

Reynolds number, Re	3000–21,000
Relative roughness height, e/D_h	0.022–0.04
Relative roughness pitch, P/e	4.5–10
Groove position to pitch ratio, g/P	0.3–0.6
Chamfer angle, ϕ	5–30°

150 mm wide and 30 mm deep and is fabricated from plywood panels of 19 mm thickness. The test section is 1200 mm long and has a cross section of 150 mm width × 30 mm depth. The entry and exit lengths were 800 mm and 600 mm, respectively. It may be noted that ASHRAE Standard 93–77 recommends minimum entry and exit length of $5\sqrt{WH}$ and $2.5\sqrt{WH}$, i.e. 336 mm and 168 mm, respectively. Consequently, the flow can be assumed to be fully hydraulically developed in almost the entire test section. An electric heater having a size of 1200 mm × 150 mm was fabricated by combining series and parallel loops of heating wire wound on asbestos sheet, to provide constant surface heat flux. The backside of the heater is insulated with 50 mm glass wool and 19 mm plywood panels to minimize the heat losses. The absorber plate is 6 mm thick aluminum plate with integral rib roughness prepared on its bottom side by machining (i.e. on top broad side of the air flow rectangular duct) as shown in Fig. 2. The topside of the entry and exit section of the duct is covered with smooth commercial available 12 mm plywood panels. The mass flow rate of air through the duct is measured by means of a calibrated orifice meter (calibrated against a standard Pitot tube) in the flow line connected with an inclined manometer, and the control valve provided to regulate the flow. The coefficient of discharge of the orifice plate having the mean value of 0.612 with

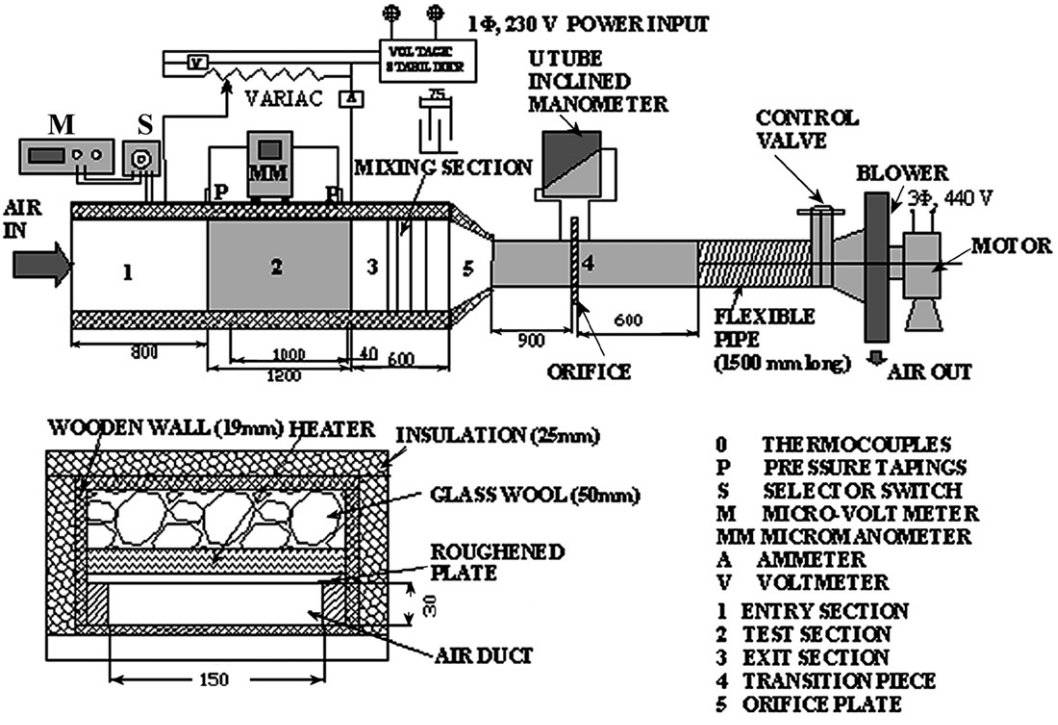

Fig. 2. Experimental set-up.

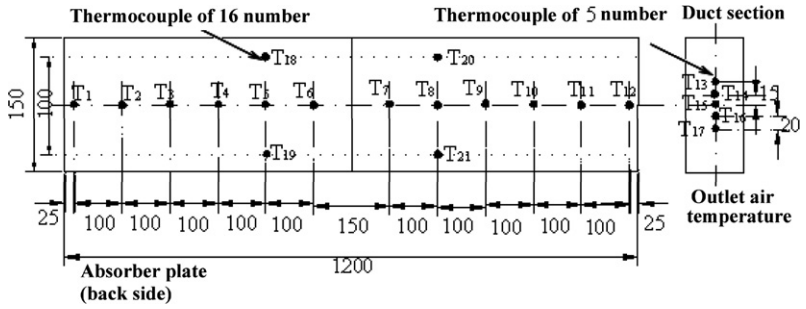

Fig. 3. Location of thermocouples on the absorber plate.

standard deviation of $\sigma = \pm 0.005$ have been used during computation. The copper-constantan of 0.3 mm diameter (24 SWG) thermocouples have been used to measure the average air and absorber plate temperatures at different locations as shown in Fig. 3. The thermocouples output is fed to a digital voltmeter through a selector switch and is used to indicate the output of the thermocouples in °C. The temperature measurement system is calibrated to yield temperature value within ±0.1 °C. The pressure drops across a 1000 mm length of test section is measured by a micro-manometer of ACIN–Betz type, having a least count of 0.1 Pa.

3.2. Experimental procedure

The test runs to collect relevant heat transfer and flow friction data under steady state conditions were conducted. Sixty-one numbers roughened surfaces of varying geometries have been used for the study in addition to a smooth duct for which data under similar conditions have been collected for the purpose of comparison with roughened ducts. Eight values of flow rates were used for each roughened surface at a fixed heat flux. It takes about 2–3 h to attain a steady state before the data were recorded. The following parameters were measured:

(i) Temperatures of the heated plate at 16 points (12 along axial direction and four in span wise direction).

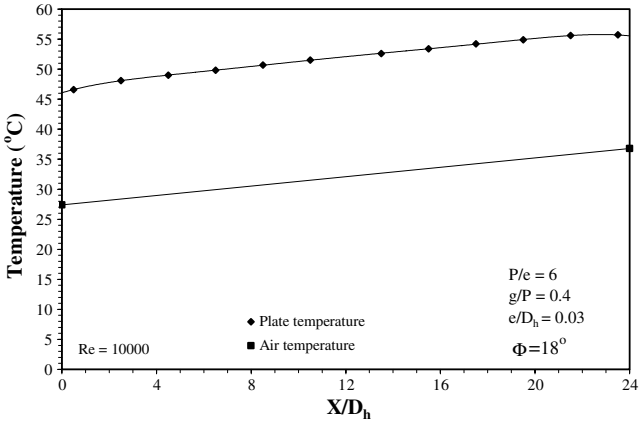

Fig. 4. Plate and air temperature profile along the length of the test duct.

(ii) Inlet air temperature.
(iii) Outlet air temperature at five points in the span wise direction of the duct (Fig. 3).
(iv) Pressure drop across the test section recorded under adiabatic (without heating) condition.
(v) Pressure difference across the orifice meter.

Fig. 4 shows the typical variations of plate and air temperatures along the length of the roughened test duct. As the heater maintains constant surface heat flux, the longitudinal distribution of the air temperature has been represented as a straight line connecting the measured mean values of temperatures at the inlet and the exit of the duct. For all the plates, the span wise plate temperature has been found to be nearly uniform with a deviation of ±0.5 °C. After a downstream distance, ranging from 5 to 6 hydraulic diameters, the gradient of plate temperature has been found to be nearly constant as can be seen from Fig. 4, indicates establishment of the thermally fully developed flow. It has been found that the departure of plate temperature from fully developed constant gradient line is small and its effect on the average value of mean plate and mean bulk air temperature difference that is $T_{pm} - T_{fm}$, can be neglected. The drop in the plate temperature near the end section appears to be due to the end effect. This effect observed here is similar to that observed by Gupta [3] and Karwa et al. [5].

4. Data processing

Mass flow rate, $\dot{m}$ of air has been determined from the pressure drop ΔP_o (measured across the orifice plate, having area of cross section of the orifice plate A_o) using the following relation.

$$\dot{m} = C_d A_o \left[\frac{2\rho(\Delta P)_o}{1-\beta^4}\right]^{0.5} \quad (1)$$

The heat transfer coefficient for the test section is calculated from:

$$h = Q_u / A_p (T_{pm} - T_{fm}) \quad (2)$$

where, the heat transfer rate Q_u, to the air is given by:

$$Q_u = \dot{m} C_p (T_o - T_i) \quad (3)$$

A_p is the heat transfer area, assumed to be the corresponding smooth plate area. Since, the plate temperature changes along the stream-wise direction, the mean plate temperature designated as T_{pm}, the area weighted mean value of the experimentally obtained plate temperatures has been employed and T_{fm} is the bulk mean air temperature. The heat transfer coefficient, h, has been used to determine the Nusselt number as, ($Nu = hD_h/k$). The friction factor was determined from the measured values of pressure drop, δ_p across the test length (L_f) of 1.0 m (between two points at 640 mm and 1640 mm from inlet) using the equation:

$$f = 2(\delta p)\rho D_h/4L_f G^2 \quad (4)$$

where $G = \dot{m}/WH$ is the mass velocity of air.

The thermo-physical properties of air employed in the calculation of heat transfer and friction parameters were picked up from available tables in Duffie and Beckman [2] corresponding to average air temperature. Further, the effect of humidity on thermo-physical properties has been neglected since the relative humidity values during the experimentation were low and variation was small, ranging between 20% and 35%.

The uncertainties [6] of the values of the Reynolds number, Nusselt number and Friction factor are estimated to be ±1.05, ±2.56 and ±7.97%, respectively for $Re = 3000$ and those for $Re = 20{,}000$ are ±0.97, ±6.18 and ±1.76%, respectively.

5. Validity test

Experimentation on roughened plates was preceded by data collection on smooth rectangular duct. The values of Nusselt number and friction factor obtained from this experiment on smooth rectangular duct have been compared in Fig. 5a and b with corresponding values obtained from correlation given by Dittus and Boelter [11] and by Kakac and Shah [12] for Nusselt number and friction factor, respectively.

These correlations are given below for ready reference,

$$N_u = 0.023\, Re^{0.8} Pr^{0.4} \quad (5)$$

for $10^4 \leqslant Re \leqslant 1.24 \times 10^5$ and

$$f = (1.0875 - 0.1125\, H/W) f_c \quad (6)$$

where, f_c is the friction factor for circular duct and is given by Prandtl–Karman–Nikuradse equation [12] as

$$1/\sqrt{f_c} = 1.7372\, \ln(Re\sqrt{f_c}) - 0.3946 \quad (7)$$

for $4000 < Re < 10^7$ and the Blasius relation, for f_c in the Reynolds number range of $4000 \leqslant Re \leqslant 10^5$ is

$$f_c = 0.0791\, Re^{-0.25} \quad (8)$$

The average absolute deviations of the experimental values of Nusselt number and friction factor from those predicted by correlation has been found to be are 2.49% and 2.32%, respectively, while the maximum deviation for Nusselt number and friction factor are 3.29% and 3.43%, respectively. Thus, a good agreement between the predicted and experimental values ensures the accuracy of the experimental data collected with the present set-up.

6. Results and discussion

The effects of various flow and roughness parameters on the heat transfer and friction characteristics for flow of air in a rectangular duct are presented below. Results have also been compared with those of the smooth duct under similar flow and thermal boundary conditions to determine the enhancement in the heat transfer coefficient and friction factor.

Fig. 6a and b show the variation of Nusselt number and friction factor as a function of relative roughness pitch with fixed values of relative roughness height, chamfer angle and relative groove position. It can be seen that the Nusselt number increases with an increase in Reynolds number in all cases as expected, whereas the friction factor decreases with the increase in Reynolds number. Chamfered rib-groove duct can be seen to yield higher Nusselt number as compared to the square rib-groove duct as is evident from the comparison of such plots with that of square rib-groove roughness having relative roughness pitch of 10. Smooth conventional surface have also been plotted in this figure for the purpose of comparison. The increase in the Nusselt number and friction factor can be attributed to the more frequent shedding of vortices with the chamfer-

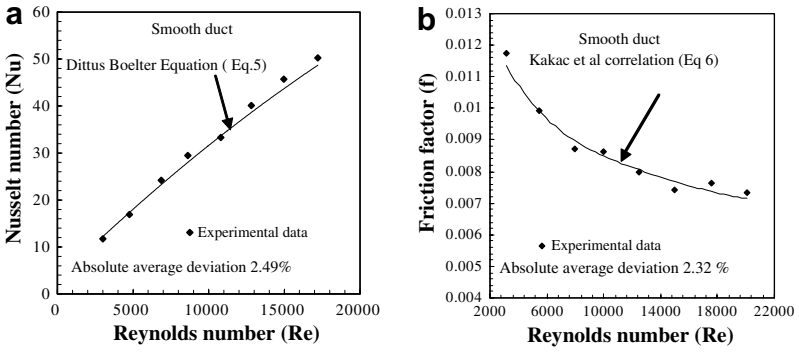

Fig. 5. (a) Nusselt number (b) Friction factor as a function of Reynolds number for smooth ducts.

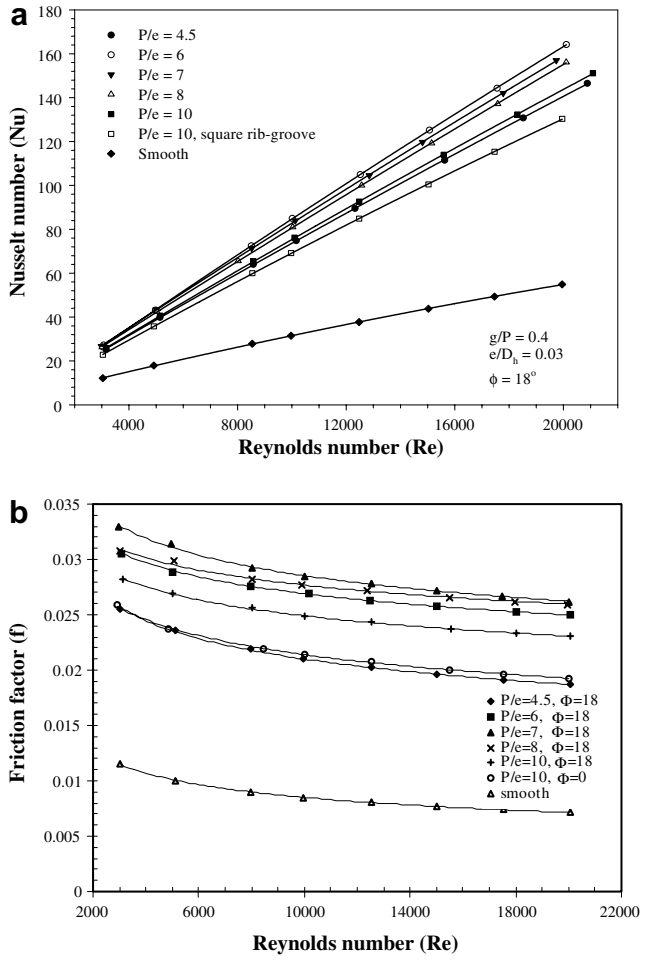

Fig. 6. (a) Nusselt number and (b) Friction factor as a function of Reynolds number.

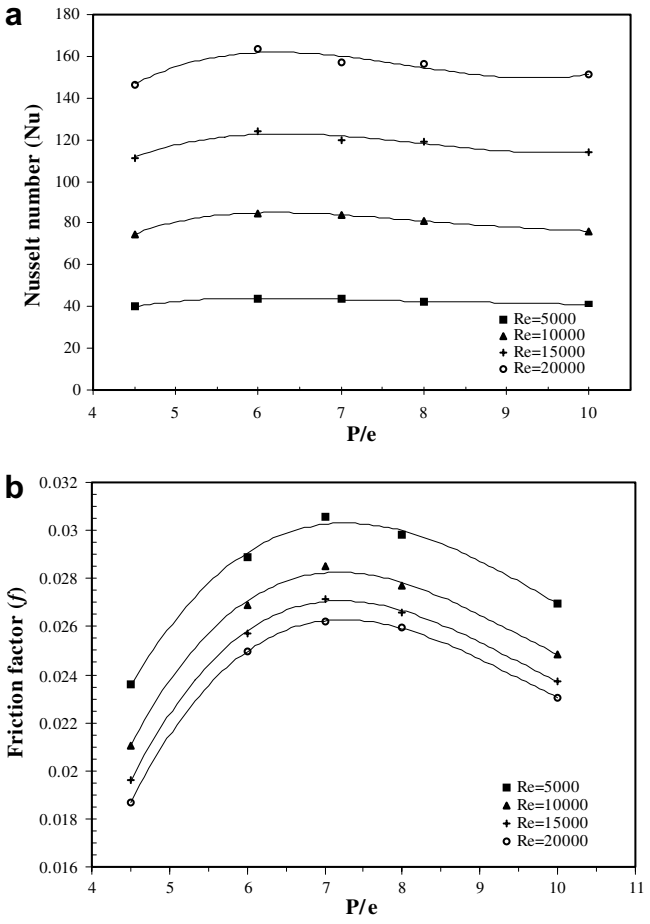

Fig. 7. (a) Nusselt number and (b) friction factor as function of relative roughness pitch (for $g/P = 0.4$, $\phi = 18°$ and $e/D_h = 0.03$).

ing of the ribs and an additional vortices created by the grooves causing greater heat removal from the surface as well as higher frictional loss.

The results presented in Fig. 6a and b are re-plotted in Fig. 7a and b to bring out the effect of relative roughness pitch on Nusselt number and friction factor. In these plots, the Nusselt number and friction factor has been plotted as a function of relative roughness pitch at few selected Reynolds numbers namely 5000, 10,000, 15,000 and 20,000. It is seen that for each Reynolds numbers Nusselt number increases with an increase of relative roughness pitch attains a maxima for relative roughness pitch of about 6 and it decreases with further increase in relative roughness pitch whereas the maxima for friction factor appears at a relative roughness pitch of about 7.

Fig. 8a and b shows the effect of relative groove position (g/P) on Nusselt number and friction factor. It can be seen that the Nusselt number and friction factor both increase with the relative groove position attains a maxima at relative groove position of about 0.4 and decrease with further increase in relative groove position.

Fig. 9a and b shows the effect of chamfer angle on Nusselt number and friction factor. It can be seen that the Nusselt number increases with increase in chamfer angle attains its maxima at about chamfer angle of 18° and it decreases with further increase in chamfer angle. While the friction factor increases with increase in chamfer angle and becomes nearly asymptotic at higher Reynolds number range. Thus, the increase in Nusselt number and friction factor with the increase in the chamfer angle from 0° to 18° can be attributed to that the increase in chamfer angle deflects streamlines towards the wall reattach earlier and causes more frequent shedding of vortices as well as greater turbulence and heat removal from the surface and more frictional loss. The observation reveals that at around 18° chamfer angle the turbulence due to the shedding of vortices reaches its maximum and further increase in chamfer angle may separate flow from the rib top surface and generates boundary layer which decreases the heat transfer and the friction factor increases monotonously due to the creation of vortices, caused by separation of flow. Fig. 10a and b shows the effect of relative roughness height (e/D_h) on Nusselt number and friction factor. It reveals that both the Nusselt number and the friction factor increase monotonously with increase in relative roughness height for all the Reynolds number, but the rise in Nusselt number is less than that of the friction factor.

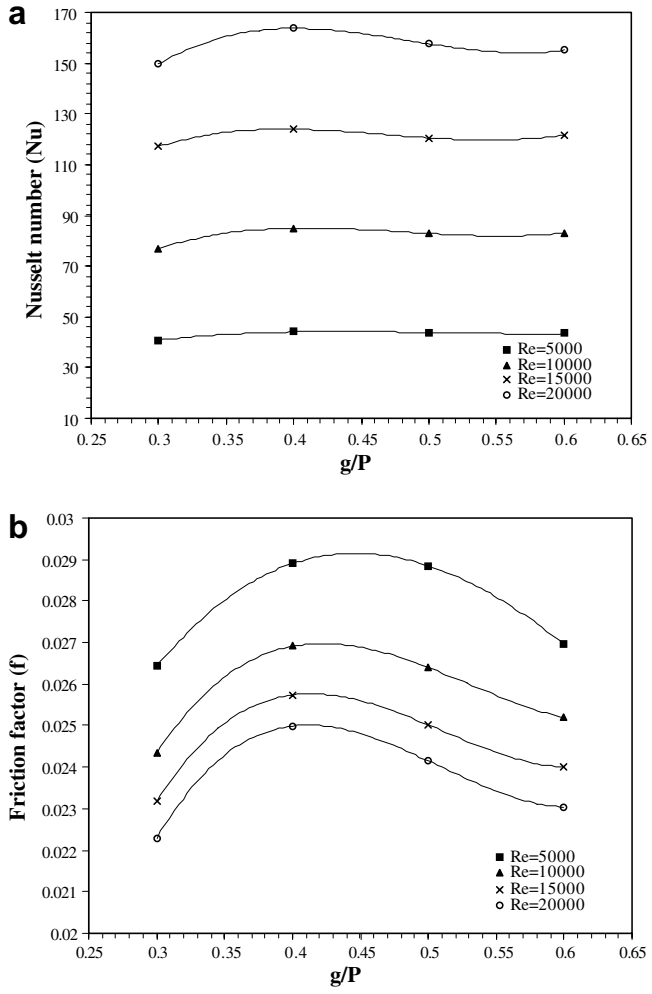

Fig. 8. (a) Nusselt number and (b) friction factor as function of relative groove position (for $P/e = 6$, $\phi = 18°$ and $e/D_h = 0.03$).

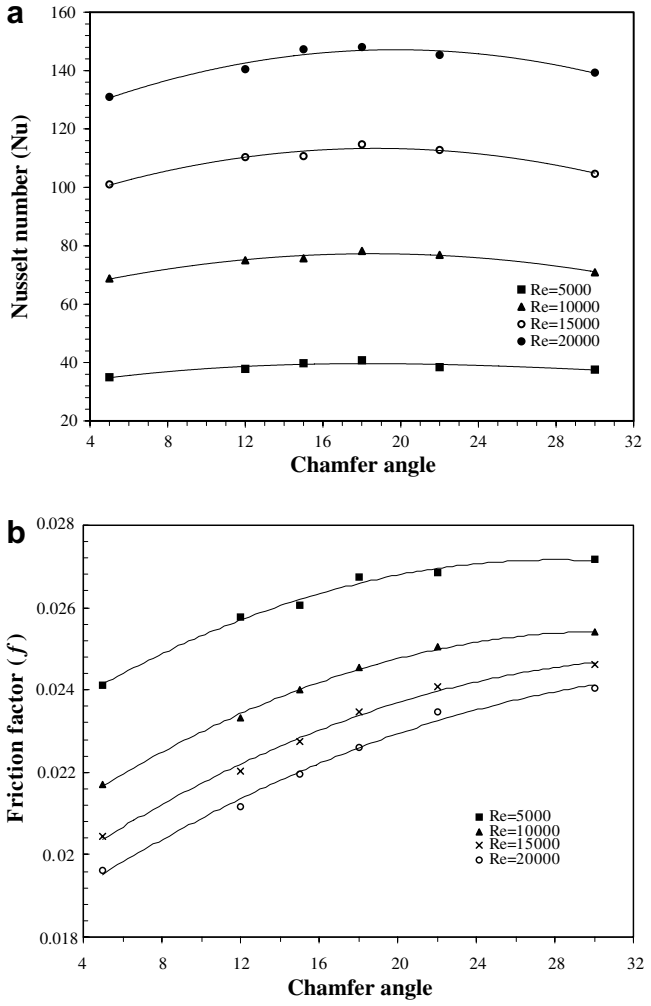

Fig. 9. (a) Nusselt number and (b) friction factor as a function of chamfer angle (for $P/e = 10$, $g/P = 0.5, e/D_h = 0.03$).

Fig. 11a and b has been drawn to depict the effect of chamfered rib-groove roughness on Nusselt number and friction factor as a function of chamfer angle for fixed values of relative roughness pitch ($P/e = 10$), relative groove position ($g/P = 0.4$) and relative roughness height ($e/D_h = 0.03$). It can be seen that there is a substantial enhancement caused as a result of providing artificial roughness in the form of chamfered groove roughness. The Nusselt number ratio enhancement achieved varies from 2.0 to 2.6 for the entire data collected from this investigation revealed that the chamfered rib-groove roughness with relative roughness pitch of 6, groove position to pitch ratio of 0.4, chamfer angle of $\phi = 18°$ and relative roughness height of 0.04 yields the maximum Nusselt number enhancement, in the order of 3.24 times that of smooth surface at Reynolds number 21,000, while the friction factor is of 3.78 times that of smooth surface.

7. Correlation for Nusselt number and friction factor

It is observed in previous discussion that the average Nusselt number and friction factor are strong functions of flow and roughness characteristics, namely flow Reynolds number (Re) and the roughness dimensions of relative roughness pitch (P/e), relative groove position (g/P) chamfer angle (ϕ) and relative roughness height (e/D_h). The functional relationship for Nusselt number and friction factor can therefore be written as:

$$\begin{aligned} Nu &= Nu(Re, P/e, g/P, \phi \text{ and } e/D_h) \\ f &= f(Re, P/e, g/P, \phi \text{ and } e/D_h) \end{aligned} \tag{9}$$

A statistical correlation is developed on the basis of regression analysis of the experimental data obtained in this work. The Nusselt number as a function of Reynolds number for the entire data corresponding to all 61 roughened plates (in all, 488 data points) of chamfered rib-groove roughened surface are plotted on log–log scale and the regression analysis to fit the straight line through these data points yields the relation between the Nusselt number and Reynolds number as:

$$Nu = A_0 Re^{0.92} \tag{10}$$

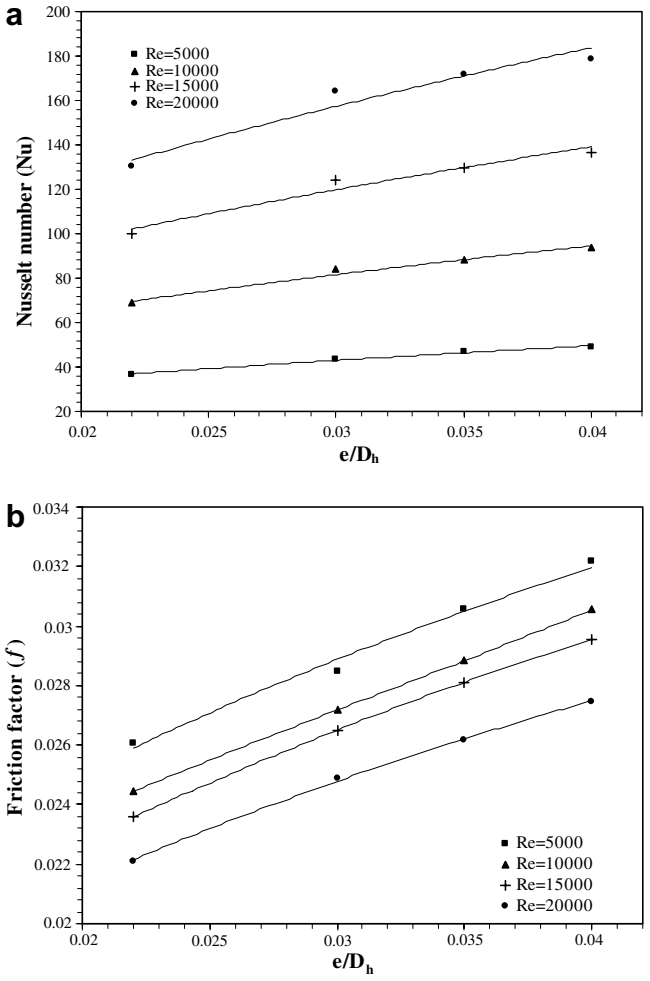

Fig. 10. Effect of Relative roughness height on (a) Nusselt number and (b) friction factor (for $P/e = 6,\ g/P = 0.4, \phi = 18^\circ$).

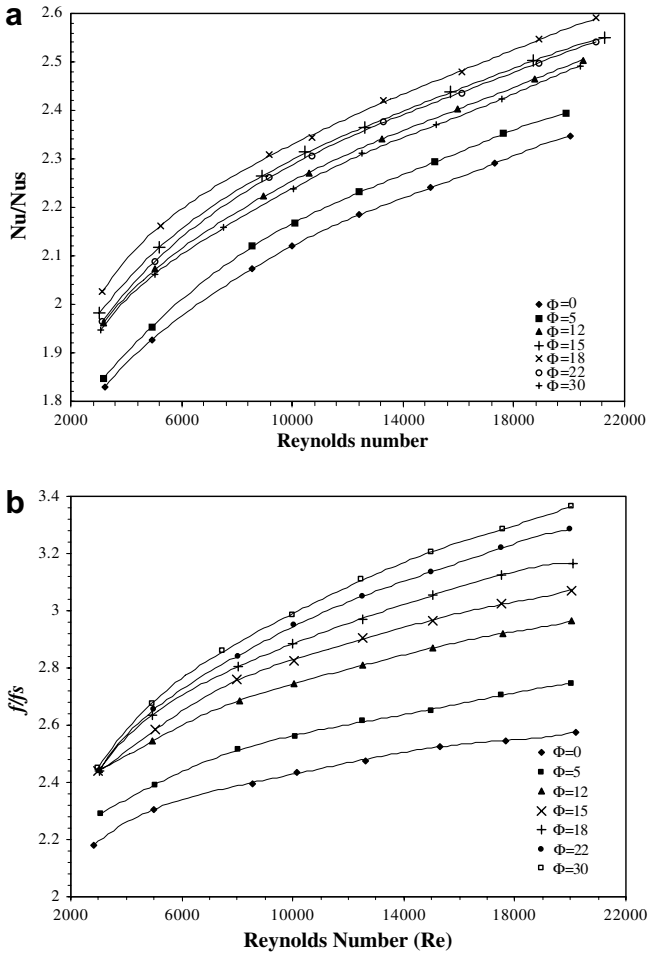

Fig. 11. (a) Enhancement ratio and (b) friction factor ratio as function of Reynolds number (for $P/e = 10,\ g/P = 0.5, e/D_h = 0.03$).

The coefficient A_0 in Eq. (10) is dependent on other influencing parameters e.g. relative roughness height (e/D_h), relative roughness pitch (P/e), chamfer angle (ϕ) and relative groove position (g/P). Now in order to find out the dependence on relative roughness height of the rib, the value of $Nu/Re^{0.92}$ is plotted as a function of e/D_h on log–log scale. A regression analysis to fit a straight line through data point's yields;

$$Nu/Re^{0.92} = B_0(e/D_h)^{0.52} \tag{11}$$

The coefficient B_0 in Eq. (11) is a function of other influencing parameters e.g. $P/e, \phi$ and g/P. In order to get the dependence of Nusselt number on chamfer angle ϕ, has been plotted as a function of chamfer angle ϕ, on log–log scale. The regression analysis to fit a quadratic curve through the data points yields the relation in the form,

$$\ln[Nu/Re^{0.92}(e/D_h)^{0.52}] = \ln C_0 + C_1 \ln\phi + C_2(\ln\phi)^2$$

Using the coefficients of C_1 and C_2 obtain from regression and rearranging the relation yields;

$$Nu/\{Re^{0.92}(e/D_h)^{0.52}\} = C_0\phi^{1.24}\exp[-0.22(\ln\phi)^2] \tag{12}$$

where C_0 in Eq. (12) is dependent on the parameters P/e and g/P. In order to incorporate the effect of P/e on Nusselt number, the value of $Nu/\{Re^{0.92}(e/D_h)^{0.52}\phi^{1.24}\exp[-0.22(\ln\phi)^2]\}$ is plotted as a function of relative roughness pitch, (P/e). A regression analysis to fit a second order polynomial on log–log scale through these data points yields the relation as:

$$Nu/\{Re^{0.92}(e/D_h)^{0.52}\phi^{1.24}\exp[-0.22(\ln\phi)^2]\} = D_0(P/e)^{1.72}\exp[-0.46\{\ln(P/e)\}^2] \tag{13}$$

where D_0 is a function of the left out parameter, g/P and in similar way the dependence on g/P is obtained which yields the final correlation for Nusselt number as:

$$Nu = 0.00225\,Re^{0.92}\left(\frac{e}{D_h}\right)^{0.52}\left(\frac{P}{e}\right)^{1.72}\left(\frac{g}{P}\right)^{-1.21}\phi^{1.24} \times [\exp\{-0.22(\ln\phi)^2\}]\left[\exp\left\{-0.46\left(\ln\frac{P}{e}\right)^2\right\}\right] \times \left[\exp\left\{-0.74\left(\ln\frac{g}{P}\right)^2\right\}\right] \tag{14}$$

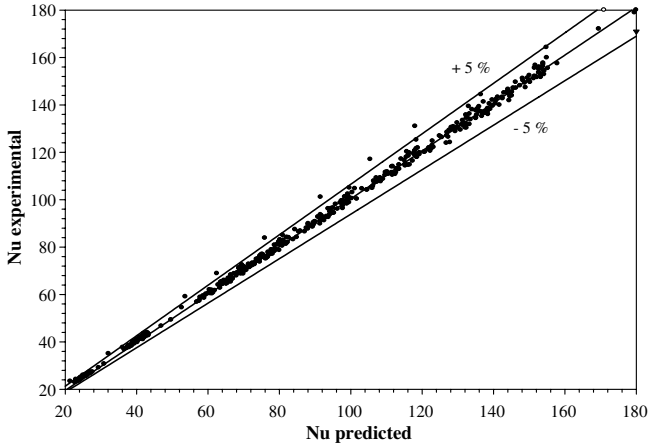

Fig. 12. Comparison of predicted vs. experimental values of Nusselt number.

The comparison between the Nusselt number obtained from experimental observation and those predicted by the correlating Eq. (14) has been plotted in Fig. 12, which shows that about 93% (456 out of 488) of the predicted data points lie within ±5% deviation lines of the experimental results. Thus, the correlation can predict the values of Nusselt number quite satisfactorily in the range of parameters investigated (viz. Re, $e/D_h, P/e$, g/P and ϕ) during the present work as shown in Table 1. The regression data for the correlation has the average absolute percentage deviation of 2.8% and the regression coefficient of 0.98. A similar procedure has been employed to develop a statistical correlation for friction factor on the basis of regression analysis of the experimental data obtained in this work corresponding to all 61 roughened plates (in all, 488 data points) having chamfered rib-groove roughness. Final correlation for friction factor that has been developed can be written as:

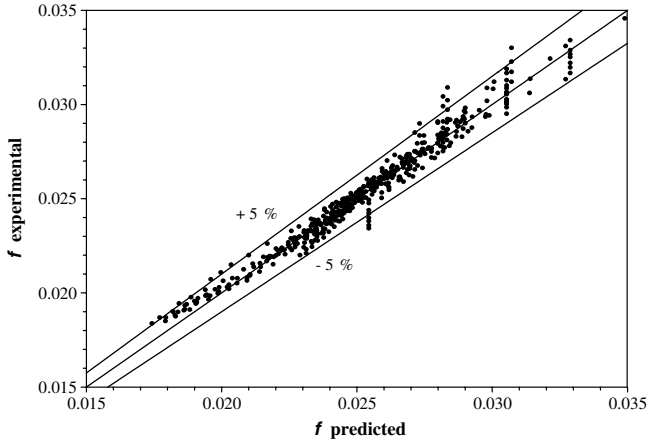

Fig. 13. Comparison of predicted vs. experimental values of friction factor.

$$f = 0.00245 Re^{-0.124} \left(\frac{e}{D_h}\right)^{0.365} \left(\frac{P}{e}\right)^{4.32} \left(\frac{g}{P}\right)^{-1.124} \times \exp[0.005\phi] \exp\left[-1.09\left(\ln\frac{P}{e}\right)^2\right] \exp\left[-0.68\left(\ln\frac{g}{P}\right)^2\right] \quad (15)$$

Fig. 13 shows the comparison of experimental values of friction factor and those predicted by the correlating Eq. (15), about 93% (455 out of 488) of the predicted data points lie within ±5% deviation lines of the experimental results. Thus, the present correlation for friction factor can predict the values quite satisfactorily in the range of parameters investigated (viz. Re, $e/D_h, P/e$, g/P and ϕ) during the present work as given in Table 1. The regression data of this correlation has the average absolute percentage deviation of 2.4% and the regression coefficient of 0.98.

8. Conclusions

Based on the experimental results of heat and fluid flow in rectangular duct with transverse chamfered rib-groove roughness on one broad wall, which is subjected to uniform heat flux the main findings are:

1. As compared to smooth surface the roughened surface can yields a maximum of about 3.24-fold and 3.78-fold increase in the Nusselt number and friction factor, respectively in the range of parameters investigated.
2. The maximum heat transfer enhancement occurs for the relative roughness pitch of 6 and relative groove position of 0.4.
3. The highest Nusselt number occurs for chamfer angle of 18° but the friction factor increase monotonously with an increase in chamfer angle.
4. Statistical correlations have been developed for Nusselt number and friction factor as a function of roughness and flow parameters. These correlations have been found to predict the Nusselt number and friction factor values with average absolute percentage deviation of 2.8% and 2.4%, respectively in the range of parameters investigated.

References

[1] D.F. Dipprey, R.H. Sabersky, Heat and momentum transfer in smooth and rough tubes at various Prandtl numbers, Int. J. Heat Mass Transfer 6 (1963) 329–353.
[2] J.A. Duffie, W.A. Beckman, Solar Engineering of thermal Processes, Wiley, New York, 1980.
[3] D. Gupta, Investigations on fluid flow and heat transfer in solar air heaters with roughened absorbers, Ph.D. Thesis, University of Roorkee, Roorkee, India, 1993.
[4] J.C. Han, Heat transfer and friction in channels with two opposite rib-roughened walls, ASME/J Heat Transfer 106 (1984) 774–781.
[5] R. Karwa, S.C. Solanki, J.S. Saini, Heat transfer coefficient and friction factor correlations for the transient flow regime in rib-roughened rectangular ducts, Int. J. Heat Mass Transfer 42 (1999) 1597–1615.

[6] S.J. Kline, F.A. McClintock, Describing uncertainties in single sample experiments, Mech. Eng. 75 (1953) 3–8.
[7] T.M. Liou, J.J. Hwang, Turbulent heat transfers augmentation and friction in periodic fully developed channel flows, ASME/J. Heat Transfer 114 (1992) 56–64.
[8] T.M. Liou, J.J. Hwang, Effect of ridge shapes on turbulent heat transfer and friction in a rectangular channel, Int. J. Heat Mass Transfer 36 (1993) 931–940.
[9] J. Nikuradse, Law of flow in rough pipes, National Advisory Committee for Aeronautics Technical Memorandum (1950) 1292.
[10] B.N. Prasad, J.S. Saini, Effect of artificial roughness on heat transfer and friction factor in a solar air heater, Solar Energy 41 (1988) 555–560.
[11] W.M. Rosenhow, J.P. Hartnett, Handbook of Heat Transfer, Mc Graw Hill, New York, 1973, pp. 7–122.
[12] Sadik kakac, R.K. Shah, W. Aung, Handbook of Single-phase Convective Heat Transfer, Wiley, New York, 1987.
[13] R.L. Webb, E.R.G. Eckert, R.J. Goldstein, Heat transfer and friction in tubes with repeated rib roughness, Int. J. Heat Mass Transfer 14 (1971) 601–617.
[14] Y.M. Zhang, W.Z. Gu, J.C. Han, Heat transfer and friction in Rectangular channel with ribbed or ribbed-grooved walls, ASME/J. Heat Transfer 116 (1994) 58–65.